Ultramicroscopy 116 (2012) 24–33

Contents lists available at SciVerse ScienceDirect

Ultramicroscopy

journal homepage: www.elsevier.com/locate/ultramic

# Oxidation state and chemical shift investigation in transition metal oxides by EELS

Haiyan Tan *, Jo Verbeeck, Artem Abakumov, Gustaaf Van Tendeloo

*EMAT, University of Antwerp, Groenenborgerlaan 171, B-2020 Antwerpen, Belgium*

ARTICLE INFO

*Article history:*
Received 25 November 2011
Received in revised form
28 February 2012
Accepted 3 March 2012
Available online 10 March 2012

*Keywords:*
Chemical shift
Oxidation state
Transition metal
Electron energy-loss spectroscopy

ABSTRACT

Transition metal $L_{2,3}$ electron energy-loss spectra for a wide range of V-, Mn- and Fe-based oxides were recorded and carefully analyzed for their correlation with the formal oxidation states of the transition metal ions. Special attention is paid to obtain an accurate energy scale which provides absolute energy positions for all core-loss edges. The white-line ratio method, chemical shift method, ELNES fitting method, two-parameter method and other methods are compared and their validity is discussed. Both the ELNES fitting method and the chemical shift method have the advantage of a wide application range and good consistency but require special attention to accurately measure the core-loss edge position. The obtained conclusions are of fundamental importance, e.g., for obtaining atomic resolution oxidation state information in modern experiments.



## 1. Introduction

Transition metals (TMs) in oxide materials are known to adopt many different oxidation states, which leads to a wide range of chemical and physical properties of the TM complex oxides [1,2]. The oxidation state, indicating the degree of oxidation of an atom, is formally the hypothetical charge that an atom would have if all bonds were 100% ionic [3]. Assuming the algebraic sum of oxidation states of all atoms in a neutral molecule/unit-cell must be zero, together with the fact that some elements almost always have certain oxidation states (due to their very high electropositivity or electronegativity, e.g., $K^+$ and $O^{2-}$), the formal oxidation state of the remaining atom (such as TMs) can be calculated in simple compounds. As such, the formal oxidation state is different from the real physical charge surrounding an atom since the bonding between TM and oxygen always has a significant covalent character. Moreover, the output of quantum mechanical calculations is a continuous electronic charge density and measuring the physical charge surrounding an atom is problematic since the outcome depends on the integration volume to which the charge is assumed to "belong" [4,5]. Although many solutions for this charge counting problem have been proposed [4–6], formal charge counting remains of fundamental importance for understanding the physics and properties of complex TM oxides.

Oxidation states can be accurately measured by redox titration techniques or thermogravimetric reduction but these techniques are material dependent and provide information averaged over the whole sample [7,8]. To obtain spatially selective information, several spectroscopic techniques are routinely used; obtaining valency information from the shape of the excitation spectra of TMs in e.g., X-ray absorption spectroscopy (XAS) [9–13]. In electron energy-loss spectroscopy (EELS), a considerable amount of publications exist linking TM oxidation states to the detailed shape of the $L_{2,3}$ ($2p \rightarrow 3d$) excitation edge [14–30]. The ability of EELS to obtain oxidation state information at atomic resolution when combined with scanning transmission electron microscopy (STEM) has drawn much attention in recent years [31–34]. This quantitative and spatially resolved analytical method for investigating TM oxidation states is of great interest for catalytic [35], mineralogical [23,24,36] and electro-chemical [37,38] applications. The discovery of 2D materials, in particular, having conducting (or superconducting [39]) electron gas [40] at the interface between two insulating materials dramatically increased the interest in measuring the oxidation state of TM cations with high spatial resolution.

In spite of this great potential, there are several restrictions in linking the detailed shape of EELS excitation edges to the oxidation state. Several procedures exist, and undoubtedly the most popular is a procedure called the white-line ratio or $L_{2,3}$ ratio method. In this method, the integral intensity ratio of the $L_3$ ($2p_{3/2} \rightarrow 3d$) and $L_2$ ($2p_{1/2} \rightarrow 3d$) excitation peaks of a TM is correlated to its formal oxidation state [25,36,37,41–43]. Although this method was successful in determining the oxidation states of Mn and Fe in some minerals in a limited oxidation state range [23,24,36,44], it is experimentally and theoretically clear that the white-line ratio has no strict one to one correspondence with the oxidation state [37,45]. Especially for Fe, this

* Corresponding author. Tel.: +32 32653249.
*E-mail address:* haiyan.tan@ua.ac.be (H. Tan).

0304-3991/$ - see front matter © 2012 Elsevier B.V. All rights reserved.
doi:10.1016/j.ultramic.2012.03.002

relation is not monotonic, making unambiguous oxidation state determination difficult. On top of this, the method is dependent on sample thickness and on the exact procedure which is used to measure the white-line intensities [23,34,37,44].

Besides that, the excitation edge energy position of the TM is also correlated to its oxidation state. In general, the excitation edges shift to a higher energy-loss for a higher oxidation state [9,10,17,19,43,46,47], which is called chemical shift [48]. Enormous efforts have been put into correlating the K edge energy position of TMs to their formal oxidation states or effective ionic charge with XAS in the past century [9,10,49,50]. Wong et al. revealed a linear relation between the threshold of the V–K edge of V oxides and its formal oxidation state [9] and a monotonic relation is also proposed for Mn oxides by Gilbert et al. [10]. However, Tromp et al. concluded that no direct relation exists between Cr oxidation state to its K edge position when different ligands are involved [51]. This could be because the K edge is mainly related to bond distance and coordination number, where L edges provide information about the oxidation state and symmetry of the coordination environment of the 3*d* TM ions [10,15,52].

Garvie et al. reported the high similarity of Mn-L edge energy-loss near-edge structures (ELNES) for different compounds with the same Mn formal oxidation states of 2+, 3+ and 4+ [16]. Afterwards, the L edge ELNES of TMs has successfully been used to determine their oxidation states by direct comparison or ELNES fitting to reference spectra [11,14,18,29,31,32,53,54]. However, in those EELS experiments, the absolute energy of the spectroscopic edges is uncertain due to primary energy drift and calibration problems [14,17,19,43,55] and hence absolute chemical shift information is typically lost. In spite of these problems, Daulton et al. carefully measured the position of the Cr-$L_3$ peak maximum and found no direct relation to the oxidation state [19] using a manual double checking of the position of the zero-loss peak. This is likely due to the fact that the $L_3$ peak maximum is strongly affected by its ELNES and hence by oxidation state, coordination geometry and spin states [19,52,56]. The peak *threshold* position, on the other hand, may still be correlated to the formal oxidation state and deserves a systematic investigation.

Potapov et al. developed a method to automatically measure the low-loss spectrum and high-loss spectrum subsequently [55]. Consequently the absolute core-loss peak position can be tracked [57]. In the present paper, this method is further improved and systematically applied to a wide group of V/Mn/Fe oxides aiming at revealing the relation between the oxidation states of these TMs and their EELS spectra. The large set of data allows us to take a critical look at the correlation between specific spectral features and the oxidation state of TMs. This work can serve as a reference to interpret modern spatially resolved EELS data [31,32].

## 2. Materials and methods

EELS experiments were performed using a JEOL 3000F microscope equipped with a Gatan GIF2000 1 K Phosphor spectrometer system operating at 300 kV. The spectrometer is set to an energy dispersion of 0.05 eV/channel to obtain the best energy resolution at the zero-loss peak (0.9 eV) and precision of the core-loss peak position (0.05 eV). EELS spectra were acquired at magic angle conditions for the $L_{2,3}$ edge of the TMs (collection angle: 1.1 mrad for Mn oxides and Fe oxides, 0.9 mrad for V oxides) to avoid anisotropy effects of the sample playing a role in the ELNES [58,59]. The convergence angles are approximately 0.85(5) mrad for the Mn/Fe spectra and 0.63(5) mrad for the V spectra.

In order to precisely and systematically measure the absolute core-loss edge position, an automated acquisition script is developed to repeatedly acquire the low-loss and core-loss spectra of O–K and TM–$L_{2,3}$ edges consecutively (Fig. 1), which is made freely available online [60]. This method significantly improves the algorithm of Potapov et al. because no change to the condenser lens is needed which improves precision [55]. The spectra are acquired in diffraction mode and the experimental condition stay the same during the total acquisition. E.g., in the case of investigating Mn oxides, an O–K edge is acquired first with energy-loss 520 eV on the drift tube of the spectrometer. Immediately after that, three low-loss spectra are acquired with the drift tube at 0 eV and a short exposure time down to 0.03 s and these are summed up later (limited by shutter speed).

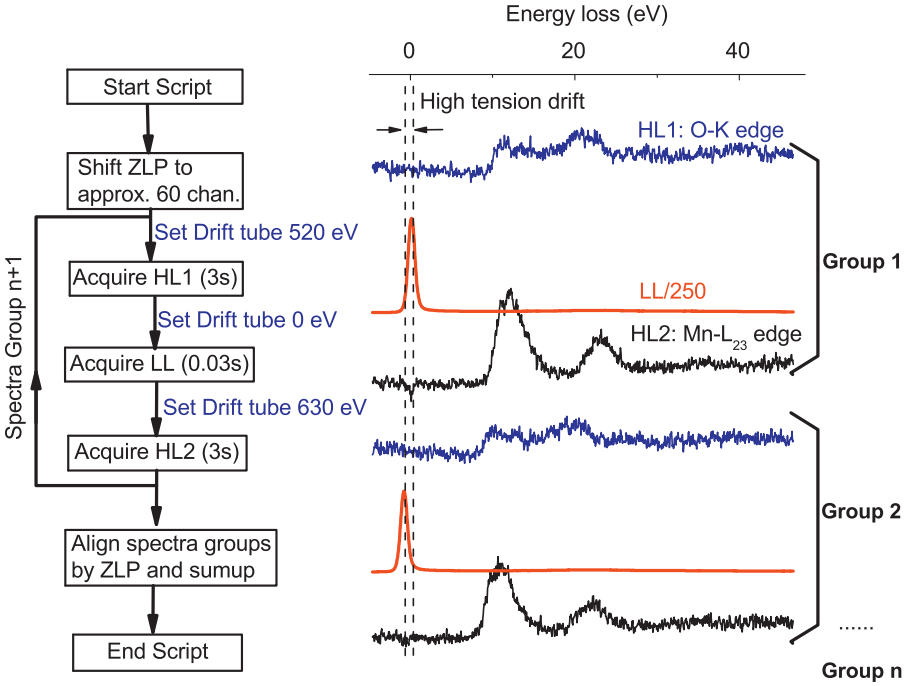


**Fig. 1.** (a) A sketch showing how the different spectra were acquired by a script to obtain an accurate absolute energy calibration and the corresponding low-loss spectrum.

The summed low-loss spectrum is used to measure the instantaneous zero-loss peak position. Then the spectrum is shifted by 630 eV to acquire the Mn-$L_{2,3}$ edge and then this procedure is repeated. To compensate for the intensity difference between zero-loss and core-loss spectra, the core-loss acquisition time is taken 100 times longer than that of the low-loss spectrum and a set of 100 spectra are acquired automatically within typically 15 min to ensure a reasonable signal-to-noise ratio (SNR) on the summed core-loss spectra. In this way the experimental conditions are kept the same for low-loss and core-loss spectra and their relative positions are precisely measured. The remaining uncertainty in edge position only depends on the calibration of the drift tube and its stability. Long term changes in the primary energy of the electrons in the microscope and drift in the spectrometer are effectively canceled in this way. All spectra are stored as spectrum images (SIs) [61] and are dispersion corrected [55], aligned according to their zero-loss peaks, and afterwards the different low-loss spectra, core-loss spectra of Mn-$L_{2,3}$ and O–K edges are summed up individually. The peak position uncertainty obtained in this way is within 0.05 eV (1 CCD channel). In the experiment, a new dark current spectrum is taken for each group of spectra in order to eliminate fixed pattern noise [57,62] which effectively increases the SNR after summation. In order to cancel residual effects of fixed pattern and gain variation, we gradually shift the position of the spectral groups over a range of 40 channels on the CCD which is later compensated by the post alignment treatment [62].

Compared to conventional EELS, this method allows acquisition of a set of nearly noise free spectra including the corresponding low-loss and core-loss spectra with precise energy calibration and good energy resolution. A relatively low beam current is used and consequently the sample suffers much less from radiation damage [63]. The fact that a series of spectra is taken over time also allows to carefully check for changes in the spectra over time due to beam damage. This method is a practical way to acquire the "complete" and relatively weak EELS signal without damaging the sample or upgrading the spectrometer to a modern dual EELS system [57,64,65]. It can also be used to measure the relative atomic ratio of two elements, whose core-loss peaks cannot be covered in a single spectrum range with a reasonable dispersion (e.g., Al–K edge at 1560 eV and O–K edge at 530 eV).

The EELS spectra of V-, Mn- and Fe-based oxides with their various oxidation states are investigated by this method in this paper. The Fe metal sample is prepared by ion milling. $Mn_3O_4$ and MnOOH nano-crystals have been provided by Li from University of Namur [66,67]. The preparation of the $YBaFe_4O_7$, $Sr_2Fe_2O_5$, $CaMnO_3$ and $SrMnO_3$ samples is described in detail in the literature [68–72]. A $BaFeO_{2.9}$ sample was prepared by annealing a stoichiometric mixture of $BaCO_3$ and $Fe_2O_3$ at 900 °C for 24 h and at 1200 °C for 48 h in air with subsequent oxidation at 900 °C for 24 h in $O_2$ flow, followed by cooling to room temperature for 72 h in an oxygen atmosphere. The oxygen content was determined from the linear relation between oxygen deficiency and lattice parameters [73].

## 3. Results and discussion

The ELNES of O–K, V-$L_{2,3}$, Mn-$L_{2,3}$ and Fe-$L_{2,3}$ edges are shown in Fig. 2 for TM oxides with different oxidation states and for metallic Fe. Their absolute energy scales are precisely calibrated with the method mentioned above and the background was removed by a power-law fitting in the pre-edge region of the spectrum. Apart from their absolute peak position, their fine structure agrees well with other publications for V [18,28,74], Mn [10,12,14,16,17,24,54,75] and Fe oxides [14,22,29,44,76] when taking into account the effect of the different energy resolution. Special care has been taken to the absence of the O–K edge prepeak in MnO which indicates that no partial oxidation occurs at the surface of the sample [10,14,75]. For $Mn_3O_4$, the $L_3$ edge appears to be split and the intensity ratio of the split peaks was

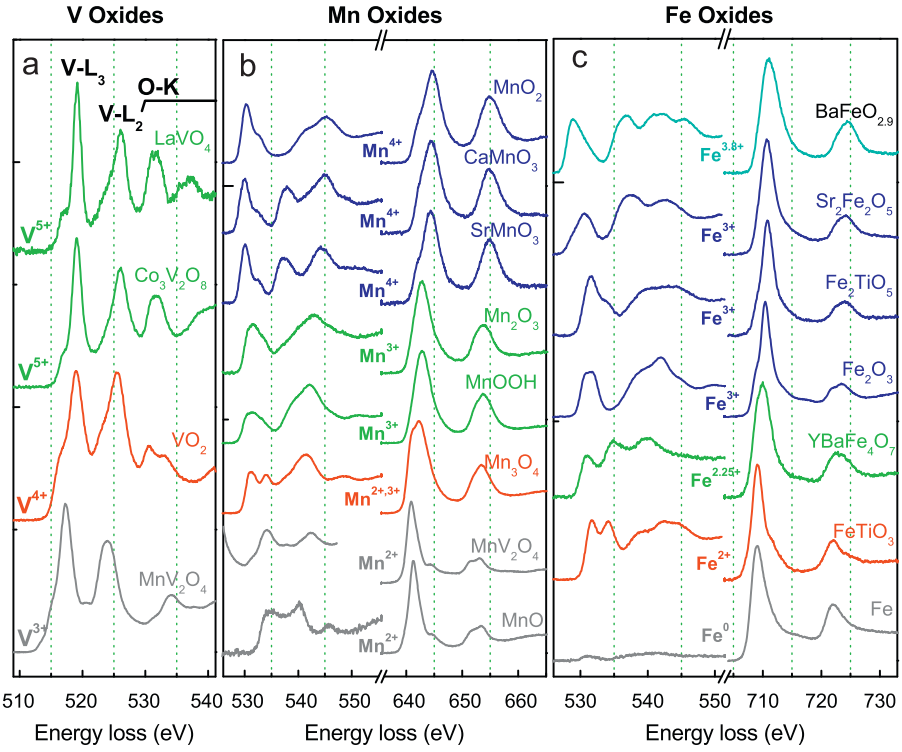


**Fig. 2.** The ELNES of vanadium, manganese and iron $L_{2,3}$ edges together with their O–K edges from oxides sorted by their TM oxidation state. The energy scale is precisely calibrated with the method described in the text.

found to be the same with the well-crystalized hausmannite mineral [16,31]. Although MnOOH is known to decompose to $Mn_2O_3$ in vacuum at 250 °C [8], its O–K ELNES remains different from our $Mn_2O_3$ reference, which implies that MnOOH is stable under our illumination conditions. However, the V-$L_{2,3}$ ELNES of $LaVO_4$ is observed to change with time in the spectrum series. Hence, only the first few spectra were summed up and are shown in Fig. 2a, whose ELNES agrees with the literature [18].

For Mn ions with the same oxidation state, the ELNES looks very similar for different compounds at the available energy resolution (Fig. 2b), which agrees with the previous observations by Garvie et al. [16]. A similar phenomenon is observed in V and Fe oxides here (Fig. 2a and c). More importantly, we observe that the ELNES peak of the V, Mn and Fe in the same oxidation state is at nearly the same energy position. In general, the position of the V/Mn/Fe-$L_{2,3}$ edge systematically shifts to higher energy-losses for higher oxidation states, which agrees with the general chemical shift rule [15,46,48] and references [14,22,24,29,75]. The O–K edge onset position of V oxides is difficult to observe since it overlaps with the continuum region of the V-$L_{2,3}$ edge. Apart from that, the O-K edge also shows a considerable shift of the onset position, which cannot be unambiguously revealed from conventional EELS without accurate energy scale calibration. As a trend, the O–K onset energy *decreases* when the TM oxidation state *increases* (Fig. 2). However, it is interesting to point out that the O–K edge onset of $Sr_2Fe_2O_5$ is much lower than that of the other $Fe^{3+}$ compounds. The Mn-$L_2$ peaks from Mn oxides are also relatively more intense for higher oxidation states, indicating a decrease of the $L_3/L_2$ white-line ratio.

### 3.1. White-line ratio method

Undoubtedly the most popular and common method to relate EELS spectra to the oxidation state is based on the anomalous $L_3/L_2$ white-line ratio being different from 2:1 as roughly explained by the 3*d* spin–spin coupling [48,77,78]. It is reported that the white-line ratio of TMs has its maximum for the $3d^5$ electronic configuration [37,45,79], which is the electronic configuration of $Mn^{2+}$ for the Mn oxides and $Fe^{3+}$ for the Fe oxides. It is also well known that the spin state of the TM also strongly affects the white-line ratio [56,80–82].

The white-line ratio can be quantitatively calculated with various empirical algorithms and parameters, leading to various relations between this ratio and the oxidation state [14,19,20,23,24,34,37,43,83–85]. In this paper, the continuum contribution to the EELS excitation edge of the TM is subtracted by a Hartree–Slater cross section [14,34,86] (Fig. 3a), since we essentially want to measure deviations from the neutral atom cross section. To minimize the systematic error from peak position and shapes, the $L_3$ edges are first aligned to the same energy-loss by cross correlation. Subsequently, the Hartree–Slater cross section is scaled to a window in the continuum range and is subtracted (Fig. 3a). The $L_3$ and $L_2$ peaks intensity is obtained by integrating the remaining intensity in a given window width.

The thickness dependence of the white-line ratio method is studied by EELS at scanning transmission electron microscopy mode (STEM–EELS) on the edge of a $Mn_3O_4$ octahedral particle [31,66] (Fig. 3b). The thickness is calculated from the corresponding low-loss spectra acquired simultaneously. The white-line ratio from the untreated spectra clearly increases with sample thickness. The ratio

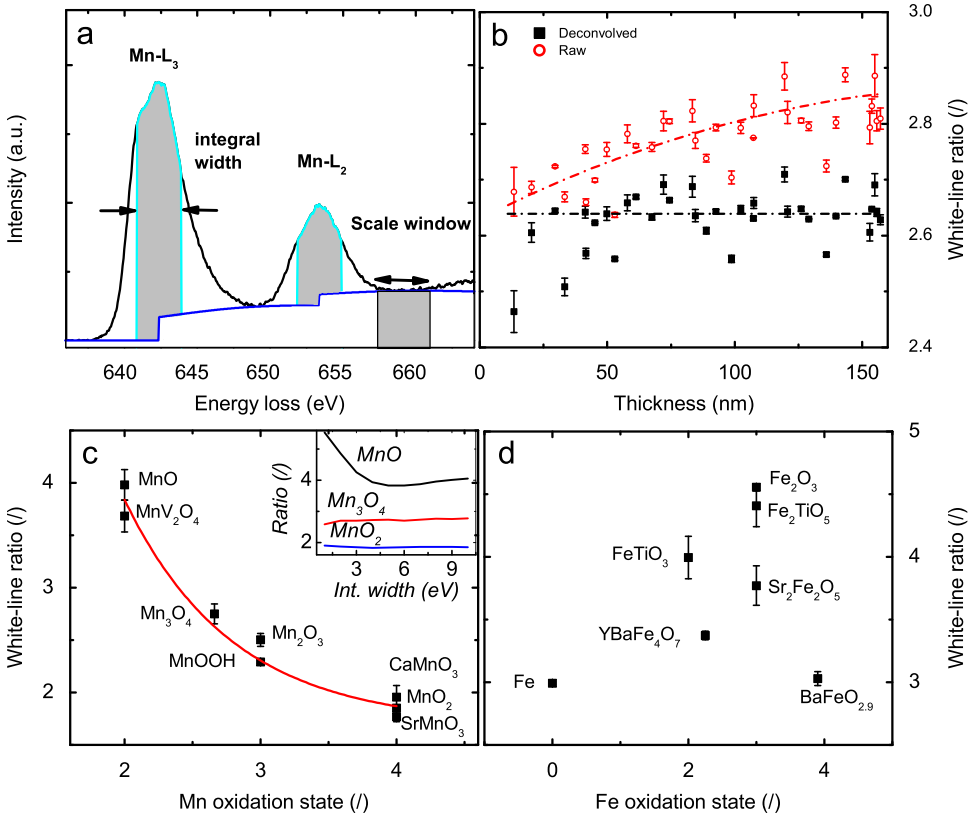


**Fig. 3.** (a) The spectral windows used to calculate the white-line ratio for a typical Mn-$L_{2,3}$ edge. (b) The Mn white-line ratio dependence (before and after deconvolution) on sample thickness for a $Mn_3O_4$ octahedron nanoparticle. The white-line ratio without deconvolution shows a strong bias effect with sample thickness while the one with multiple scattering deconvolution is relatively constant. The drop at the left side of the deconvolution curve is because of deconvolution artifacts due to the strong zero-loss peak and weak plasmon peak at thin sample regions, leading to shutter induced artifacts in the zero-loss peak. The inset of (c) shows the Mn white-line ratio dependence on the integration width. (c) and (d) The white-line ratio of Mn and Fe oxides obtained with an integration width of 8 eV after multiple scattering removal. The standard deviation is obtained from measuring different regions of the same compound.

increases from 2.65(5) to 2.85(5) when the thickness increases from $t/\lambda = 0.3$ to 1. This shows that a strong bias effect is present in this method as a function of thickness. This increase of the white-line ratio with respect to sample thickness can be understood as multiple scattering which transfers intensity from both $L_3$ and $L_2$ peaks into the continuum region. This will lead to an overestimate of the continuum and an underestimate of both the $L_3$ and $L_2$ intensities which makes the $L_3/L_2$ ratio rise. The effect of thickness can be reduced by the removal of multiple scattering with Fourier ratio deconvolution [30,48]. After this procedure, the white-line ratio becomes relatively constant of 2.63(7), which also agrees with the white-line ratio obtained from a thin sample region (Fig. 3b). This shows that deconvolution is absolutely necessary when applying the white-line ratio method, contrary to what was stated by Varela et al. [34]. Care has to be taken however as the deconvolution procedure will deteriorate the SNR of the spectrum and may bring artifacts especially in the thin areas (Fig. 3b). All spectra in this paper are multiple scattering removed for the white-line ratio calculation.

As demonstrated in the inset of Fig. 3c, the white-line ratio also sensitively depends on the size and position of the integration window due to the subtle differences in the ELNES shape of the different compounds. The Mn-$L_3$ edge of MnO consists of a sharp peak with full width at half maximum (FWHM) of 2 eV and its $L_2$ edge is a broad plateau (Fig. 2b). Because of this, the white-line ratio decreases from 5.4 at 1 eV integration window width to 3.8 at 6 eV integration window width and again increases to 4.1 at 10 eV window width (Fig. 3 c(inset)). For $MnO_2$ and $Mn_3O_4$, both the $L_3$ and $L_2$ peaks are broad peaks with similar width. Consequently, their white-line ratios depend only slightly on the integration width. This dependence on window width makes this method difficult to apply. For further calculations, we choose a window width of 8 eV to minimize this dependence. The results are listed in Tables 1 and 2 for Mn and Fe oxides, respectively.

Attempting the white-line ratio method for V oxides is problematic in view of the overlap of the V-$L_{2,3}$ edge and the O–K edge. The V-$L_{2,3}$ edge (520 eV and 513 eV) is immediately followed by the O–K edge (532 eV) which makes it difficult to remove the V continuum contribution correctly and therefore we omit the vanadium oxides from the discussion on the white-line ratio.

Fig. 3c shows the Mn white-line ratio with the standard deviation calculated from repeating measurements from different areas of the same compound. Because of the various methods and parameters applied in the literature, it is hard to directly compare our values with the literature data [14,19,26,30,34,54,75,85]. Nevertheless, the trends are similar for the Mn oxidation state except Ref. [54]. We can fit our results to an exponential function (Fig. 3 c(red))

$$R_{Mn} = A \cdot \exp(-V_{Mn}/t) + y_0 \quad (1)$$

with $A = 24(9)$, $t = 0.83(11)$ and $y_0 = 1.64(8)$.

The Fe white-line ratio does not show a monotonic relation with respect to its Fe oxidation state (Fig. 3d) because the ratio reaches its maximum at the electronic configuration $3d^5$ ($Fe^{3+}$). Such non-monotonic behavior makes it ambiguous to quantify the Fe oxidation state directly from the Fe white-line ratio. Most importantly the function seems to be multi-valued for $Fe^{3+}$ well above the error bar of the measurements (Fig. 3d). The white-line ratio of $Sr_2Fe_2O_5$ is considerably lower than that of the other $Fe^{3+}$ samples (Fig. 3d). As $Fe^{3+}$ in $Sr_2Fe_2O_5$ is also reported to be in a high spin state as all other Fe compounds we have been discussing here [87], this discrepancy implies that other factors, apart from the nominal Fe oxidation state, e.g., coordination geometry, also strongly affect the Fe white-line ratio in some cases [15].

The white-line ratio method depends in a sensitive way on the chosen settings and comparison with published data is difficult [22,23,34,88]. When applying different parameters, different fits other than Eq. (1) can be derived but the general trend remains. Also note that the white-line ratio is a nonlinear function of the formal Mn oxidation state. Hence, special care has to be taken for mixed valence compounds with cations having different oxidation states. In this case, Eq. (1) will not lead to the correct average valence from the measured white-line ratio because of this nonlinear dependence.

As an example, the Mn cation in $Mn_3O_4$ is known to consist of 1/3 $Mn^{2+}$ and 2/3 $Mn^{3+}$. They are ordered over the tetrahedral and octahedral positions in the spinel type structure [31,66]. As a simple model one could imagine that the experimental Mn-$L_{2,3}$ edge would be a simple superposition of $Mn^{2+}$ and $Mn^{3+}$ spectra ($MnO + Mn_2O_3$). Applying the white-line ratio relation (Eq. (1)) on $Mn_3O_4$ would lead to an Mn average valence of +2.57(6) while we know that its average valence is +2.67. Knowing that we have a mixture of $Mn^{2+}$ and $Mn^{3+}$ we can also use a linear relationship to link the observed white-line ratio to the oxidation state leading to an estimate of +2.69(6) which is much closer to the expected value. This nonlinear effect was not discussed and was typically ignored in the previous literature [23,24,83].

This also shows that some knowledge of the sample (singular valence state or mixed valence state) is necessary to guide the valence calculation from the white-line ratio method. Without prior knowledge, one cannot tell the difference between a proper mixture of $Mn^{2+}/Mn^{4+}$ state and a singular $Mn^{3+}$ state since the total white-line ratio could be the same [89]. This situation can be further complicated if more than two unknown oxidation states are present [11,85,89]. This is specially difficult in the case of spatially resolved STEM–EELS on inhomogeneous materials (e.g., minerals), where several compounds may overlap with each other in the direction of the fast electrons [23,24,83,89].

Besides, the white-line ratio method is not applicable for V oxides due to its $L_{2,3}$ edge overlapping with the O–K edge and for Fe oxides due to non-monotonic relation with the Fe oxidation

**Table 1**
Mn-$L_3$, O–K edge onset energy, Mn-$L_{2,3}$ edge white-line ratio and Mn nominal oxidation states of the investigated manganese oxides.

| Oxid. state | Phase | Mn onset | O onset | Mn-$L_{2,3}$ ratio (8 eV) | Struc. ref. (ICSD No.) |
|---|---|---|---|---|---|
| +2 | MnO | 639.12(5) | 532.00(5) | 3.98(15) | 30520 |
| | $MnV_2O_4$ | 639.06(5) | – | 3.68(15) | 30520 |
| +3 | MnOOH | 639.91(5) | 529.05(5) | 2.29(2) | 84949 |
| | $Mn_2O_3$ | 639.94(11) | 529.21(10) | 2.50(6) | 61271 |
| +4 | $MnO_2$ | 640.72(3) | 528.55(14) | 1.85(2) | 73716 |
| | $SrMnO_3$ | 640.79(5) | 528.41(9) | 1.77(5) | 86645 |
| | $CaMnO_3$ | 640.83(10) | 528.02(14) | 1.95(11) | 202615 |
| +2, +3 | $Mn_3O_4$ | 639.31(4) | 529.44(3) | 2.75(10) | 77478 |

**Table 2**
Fe-$L_{2,3}$, O–K edge onset energy, Fe-$L_{2,3}$ edge white-line ratio and Fe nominal oxidation states of the investigated iron oxides.

| Oxid. state | Phase | Fe onset | O onset | Fe $L_{32}$ ratio (8 eV) | Struc. ref. (ICSD No.) |
|---|---|---|---|---|---|
| 0 | Fe | 706.88(11) | – | 2.99(1) | 631724 |
| +2 | $FeTiO_3$ | 706.70(4) | 529.90(12) | 3.99(17) | 30669 |
| +2.25 | $YBaFe_4O_7$ | 707.22(9) | 529.28(17) | 3.37(4) | 163145 |
| +3 | $\alpha$ $Fe_2O_3$ | 708.03(4) | 529.35(2) | 4.55(3) | 82902 |
| | $Fe_2TiO_5$ | 708.02(9) | 529.52(9) | 4.41(17) | 88380 |
| | $Sr_2Fe_2O_5$ | 708.19(6) | 527.85(24) | 3.77(16) | 51318 |
| +3.8 | $BaFeO_{2.9}$ | 708.19(3) | 527.23(9) | 3.03(6) | 153095 |

state (Figs. 2a and 3d). Other methods have to be applied in these cases.

### 3.2. Chemical shift of the TM–L edge

A chemical shift manifests itself as a displacement of the K or L excitation edge of TMs towards higher energy-loss when they are in a higher oxidation state. However, it is difficult to define the peak position quantitatively for different compounds due to a varying ELNES. Since the ELNES largely depends to a different extent on the oxidation state, spin state, coordination geometry and ligand type [15,19,52,78], it is not convincing to define the peak position as the position of its maximum [14,19], which may represent different energy transitions in different compounds. It is more common to consider the edge onset of an EELS edge as the inflection point of the initial rise at the threshold [26] as demonstrated in Fig. 4a. This represents the lowest excited energy level allowed for a given edge. To take into account the presence of possible weak prepeaks and to suppress the effect of noise, the energy-loss where the edge reaches 10% of its maximum is taken as the edge onset in this paper. Note that the onset position will be different if another threshold is chosen but in most cases the edge onset follows a similar trend for different thresholds. Choosing different thresholds leads to slight changes in the *relative* edge onset energies for different compounds, but this effect is smaller than the precision of the peak position (0.05 eV) as shown in (Fig. 4 a(inset)) for thresholds between 5% and 25% of the peak maximum.

The obtained edge onset energies for all the investigated materials are summarized in Tables 1–3 for the Mn/Fe/V oxides, respectively. It is worth noting that the absolute energies, as displayed here, are still influenced by the calibration of the drift tube and can therefore differ $\sim 1$ eV for different instruments. However, on the other hand, the relative changes measured on the same instrument should form a reliable way of discriminating different compounds. This is proven from repeated measurements on the same sample at different times and regions.

The onset energies of the V-, Mn-, Fe-$L_3$ edge are plotted as a function of their formal oxidation states in (Fig. 4b–d). Generally speaking, these $L_3$ edge onset energies show a monotonic increase with cation oxidation state. For the V oxides, the relationship can be fitted linearly (Fig. 4b)

$$E_V = a \cdot V_V + b \tag{2}$$

with $a=1.15(4)$ and $b=510.28(16)$.

For the Mn oxides, attention has to be paid to the mixed oxidation state compound $Mn_3O_4$ which will be discussed later. Excluding this, the relation also follows a linear trend

$$E_{Mn} = a \cdot V_{Mn} + b \tag{3}$$

with $a=0.83(2)$ and $b=637.43(7)$.

The onsets of the Fe-$L_3$ edges also show a monotonic increase when Fe is more oxidized (Fig. 4d). The Fe-$L_3$ onsets of $Fe^{3+}$ compounds ($Sr_2Fe_2O_5$, $Fe_2TiO_5$ and $Fe_2O_3$) are close to each other and within the experimental error bar. This implies that the Fe oxidation state is much better associated with the Fe-$L_3$ onset than

**Table 3**
V-$L_{2,3}$ edge onset energy and nominal oxidation states of the investigated V oxides.

| Oxid. state | Phase | V onset | Struc. ref. (ICSD No.) |
|---|---|---|---|
| +3 | $MnV_2O_4$ | 513.77(5) | 109148 |
| +4 | $VO_2$ | 514.70(10) | 34416 |
| +5 | $LaVO_4$ | 515.99(5) | 155240 |
| | $Co_3V_2O_8$ | 516.09(5) | 2643 |

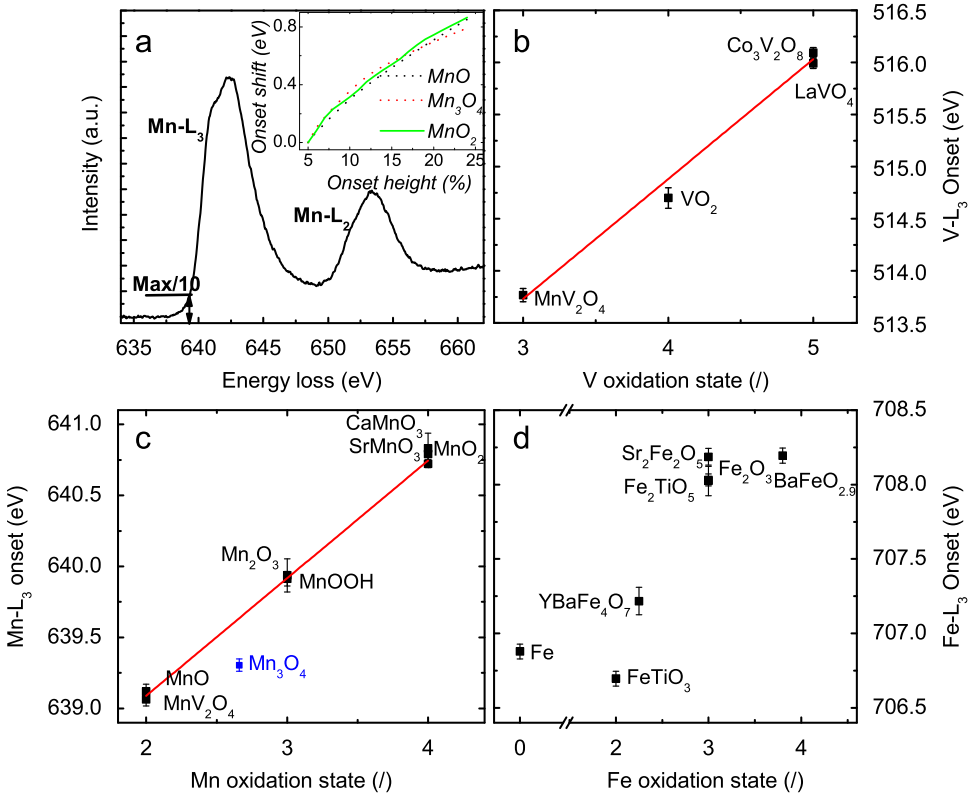


**Fig. 4.** (a) Sketch of the algorithm of extracting the Mn-$L_3$ edge onset energy. The inset shows the changes of MnO, $Mn_3O_4$ and $MnO_2$ $L_3$ onset energy when different threshold intensities are chosen. (b) and (c) V- and Mn-$L_3$ edge onset energy for different oxides shows a linear increase according to their formal oxidation state. (d) A monotonic increase with oxidation state for Fe compounds is also observed except metallic iron.

with its white-line ratio (Fig. 3d). However, the onset of $Fe^{3.8+}$ in $BaFeO_{2.9}$ is at the same level as $Fe^{3+}$. This can be explained as $BaFeO_{2.9}$ is a non-stoichiometric compound [90,91] where, to compensate the deficiency of oxygen, part of the Fe ions may be randomly reduced to the 3+ state. This implies that the $BaFeO_{2.9}$ spectrum is a linear combination of the $Fe^{3+}$ and the $Fe^{4+}$ signal. In this case, its Fe-$L_3$ edge onset is similar to that of the $Fe^{3+}$ compounds. Another indication is that the FWHM of the $BaFeO_{2.9}$ Fe-$L_3$ edge is much wider than that of the $Fe^{3+}$ compounds (Fig. 2c), implying an overlap of $Fe^{3+}$ and $Fe^{4+}$ spectra.

The absolute peak position method measures the energy-loss of excitations, which is closely related to the energy level of the inner-shell electrons and the final states [48]. This transition is not thickness dependent and the edge onset method has a much better precision with our presented routine (lower error bar). In this way, the V/Mn-$L_{2,3}$ onset energy is found to linearly relate to the oxidation state of the transition metals, which gives a straightforward way to quantify the oxidation states of V/Mn in their oxides (Fig. 4b and c). Nevertheless, due to ELNES variations, measuring the edge onset or chemical shift of the excitation edge is slightly resolution dependent.

While applying this chemical shift method, special care has to be taken with charge ordered compounds [1]. The spectrum of $Mn_3O_4$ can be thought of as the overlap of an $Mn^{2+}$ spectrum and an $Mn^{3+}$ spectrum which have peak onsets that differ by 0.83(2) eV. Analyzing the edge onset on this compound would show only the lowest onset which represents the cations with the lowest oxidation state. This is the reason why the Mn-$L_3$ edge onset for $Mn_3O_4$ is very similar to that of MnO and $MnV_2O_4$ (Table 1, Fig. 4c). This restriction largely limits the application of this method since in many cases the average oxidation state in a mixture is of great interest [11,38,89,92].

This charge ordered situation is different from that of non-integer valence compounds (e.g., $YBaFe_4O_7$ with $Fe^{2.25+}$). One could expect that when the oxidation state changes continuously to a higher valence, also the $L_3$ edge should shift to a higher energy-loss continuously. Suppose there would be a compound $Mn_3O_4$ with all identical $Mn^{2.66+}$ cations, then it would demonstrate a single Mn-$L_3$ edge with an onset at 639.64 eV rather than the overlap of $Mn^{2+}$ and $Mn^{3+}$-$L_3$ edges with an onset at 639.31(4) eV (similar as that of MnO).

Besides that, small prepeaks, which might relate to excitons under the fermi level, could be present at the onset. This will influence the estimated edge onset position [48]. One could expect that the electrical conductivity and band gaps of the materials could influence the ELNES considerably [48]. In view of the wide range of electrical properties of the materials we studied ($MnO_2$ is even a good conductor [93]), we conclude however that the observed trend with respect to oxidation state is rather insensitive to these differences.

### 3.3. O–K edge onset

It is also interesting to look at the ELNES of the O–K edges. It is clear that even though nominally all oxygen atoms have (−2) oxidation state, their ELNES and peak position can be dramatically different (Figs. 2b,c and 5a,b). The nearly 4 eV peak position shift of the MnO O–K edge to a lower energy-loss is also observed in other measurements [10,94]. This fact proves that manually aligning spectra to the O–K edge onset when absolute energy positions are not available in the experiment is not justified [21,26,34]. It also supports that the ELNES of the O–K edges are more related to the geometry of the metal–oxygen bonding rather than to the oxidation state of the TMs [15]. The data we present here profit from a very good peak position accuracy (0.05 eV) obtained by the method described above as compared to the conventional method (typically 0.5–1 eV) [14,16,19].

Although the O–K edge onset of Mn oxides seems to have a consistent relation to the nominal Mn oxidation state (Fig. 5a), one has to note the fact that since oxygen is not only bonded to the TM but also to other elements (if present), its ELNES involves the contribution from all bonds. This can be the origin of the 0.4 eV lower O–K edge onset in $CaMnO_3$ in comparison with that of $SrMnO_3$.

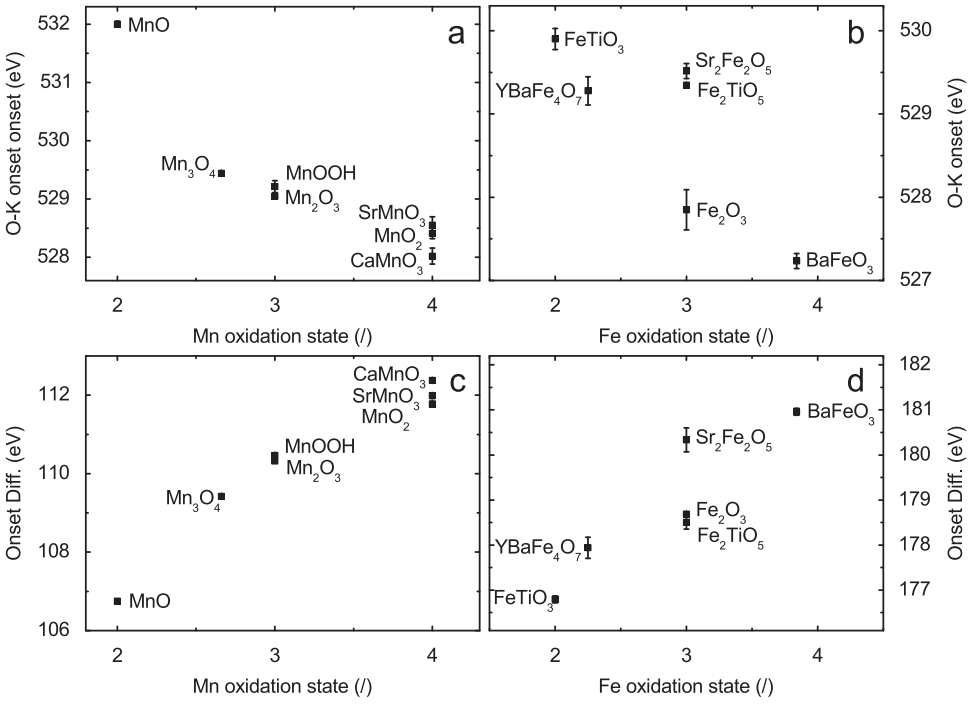


**Fig. 5.** (a) and (b) Edge onset energy of O–K edges from Mn and Fe oxides. (c) and (d) The energy onset difference between O–K edges and Mn-$L_3$ or Fe-$L_3$ edges. Note the small error bar obtained from measuring different regions which shows the superior repeatability of this method.

### 3.4. Edge onset difference

Arevalo et al. investigated the peak onset *difference* between the O–K edge and the Cr-$L_3$ edge versus the Cr oxidation state [21] thereby ruling out the need for absolute energy calibration. They assumed that both the O–K and the Cr-$L_{2,3}$ were probing the same (hybridized) final states. Therefore the onset energy difference between the O–K edge and the Cr-$L_3$ edge reflects the energy difference between the inner shell energy level of O 1*s* and Cr $2p_{3/2}$. This can be used to reliably quantify the oxidation state of TM oxides if the O 1*s* states stay the same in all Cr oxides. However, our results show that the absolute peak onset of the O–K edge in Mn and Fe oxides varies by as much as 4 eV (Fig. 5a and b) either due to the change of the O 1*s* initial state or due to changes in the final state. As such, this method would be valid only when the O 1*s* initial states remain the same in all oxides and when final state effects due to hybridization and crystal field are negligible. Besides that, the ELNES of an atom reflects the highly localized density of state (DOS), which implies that the final states at the Cr sites can be very different from the O sites [48].

Nevertheless, we apply this idea to our experimental data for the Mn and Fe compounds as shown in Fig. 5c and d, respectively. The onset difference between O–K edge and Mn-$L_3$ edge shows a monotonic increase with the Mn nominal oxidation state, which is similar with the result from Zhang et al. [54]. However, in a large oxidation state range, the increase is found to be nonlinear which is mainly because of a nonlinear decrease of the O–K edge onset (Fig. 5a). The trend is also present in Fe oxides but $YBaFe_4O_7$ and $Sr_2Fe_2O_5$ are outliers (Fig. 5d). This may be related to the fact that the K edge ELNES is much more closely related to the coordination geometry than the L edge [15,95]. So the observed anomaly might related to the fact that the Fe coordination number (CN) in $YBaFe_4O_7$ is 4 and that of $Sr_2Fe_2O_5$ is 4 and 6, while for the other compounds the CN is 6.

The edge onset difference method assumes that the oxygen and TM have the same final state, which in general is not true because the density of states are localized [48]. Although both methods seem to work to identify the oxidation states of Cr or Mn in some cases [19,21,54] (Fig. 5), too many outliers exist and application to mixed valence compounds fails because of spectral overlapping.

### 3.5. Two-parameter method

Using the fact that both the white-line ratio and the $L_3$ edge position depend in some way on the nominal oxidation state, one could also use both indicators together to estimate the nominal oxidation state from experiments. Dalton et al. analyzed the white-line ratio of a large group of Cr compounds as a function of the Cr-$L_3$ peak maximum position [19]. Different Cr compounds tend to cluster according to their nominal oxidation state. Here we adopt this method for Mn and Fe oxides (Fig. 6) but replace the $L_3$ peak maximum position by the $L_3$ peak onset position for reasons we discussed above. The Mn oxides with the same nominal Mn oxidation state cluster nicely and are well separated from different Mn oxidation state compounds (Fig. 6a). Nevertheless, the Fe oxides with different nominal oxidation states do not segregate clearly in such plot (Fig. 6b). This is because of the anomaly in the Fe white-line ratio (Fig. 3d) and the inapplicability of the chemical shift method to deal with mixed valence situation (Fig. 4d). Especially $Sr_2Fe_2O_5$ ($Fe^{3+}$) is located close to $BaFeO_{2.9}$ ($Fe^{3.8+}$) on this plot. This is again related to the observation that the white-line ratio method is not suitable for reliably estimating the Fe oxidation state (Fig. 3). So the performance of the two-parameter method is dependent on the validity of the individual methods.

The peak onset position of the Mn/Fe-$L_3$ edge versus the O-K edge is also plotted in Fig. 6c and d. All of the compounds can be well separated by regions on the plot except for $Sr_2Fe_2O_5$. But since the O–K edge involves its coordination geometry [95] and

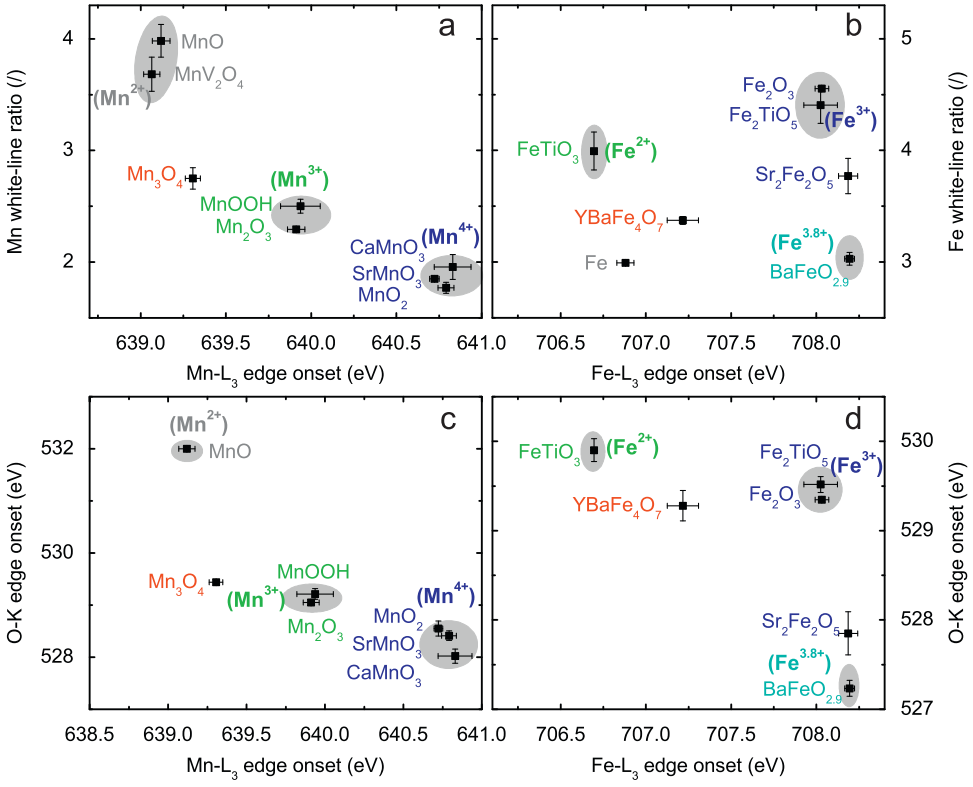


**Fig. 6.** (a) and (b) $L_{2,3}$ edge white-line ratio versus the $L_3$ edge onset for Mn and Fe in their oxides, respectively. Compounds with the same Mn or Fe oxidation state agglomerate to a certain extent. (c) and (d) Mn/Fe-$L_3$ edge onset plotted against the O–K edge onset for Mn/Fe oxides with different oxidation states.

ligand with the other cations, this method is not suited to estimate oxidation states of TMs.

### 3.6. ELNES fitting method

Garvie et al. published high resolution L edge ELNES data of $Mn^{2+}$, $Mn^{3+}$ and $Mn^{4+}$ with different coordinations and ligands [16,89,95,96]. The high ELNES similarity of the compounds with the same Mn oxidation state proves that for these compounds the ELNES is mainly dominated by the Mn oxidation state [10,16,78]. The covalence, ligand, coordination geometry, etc. mainly affect the sharpness of the subpeaks and slightly the relative height of the peaks. Gradual ELNES changes are also observed in atomic multiplet calculations when the crystal field split increases before exceeding the spin pairing energy [52,78]. When the crystal field split exceeds the spin pairing energy, abrupt changes in the ELNES can occur for the L edges [19,52,78,97]. When this happens, the white-line ratio and peak onset position can also be very different [56,78,80]. Fortunately, the fourth period TMs in their inorganic oxides are usually in a high spin state [19,56,98]. This fact provides a method to use these spectra with typical ELNES structures as references to fit spectra of unknown oxides, which typically contain a mixture of different oxidation states. This ELNES fitting method is successfully used to measure the oxidation states of V [18], Ti [53], Mn [16,31,54,94], Fe [29] and Ce [32]. It is worth to note that this method should be applied with caution to the non-integer valence compounds, whose excitation edge might be very different.

In such experiments, typically an absolute energy scale is missing although the latest dual EELS spectrometers could change that in the future [64,65]. However, as we demonstrated earlier, the chemical shift or peak position is a key ingredient in distinguishing differences in excitation edges for different oxidation state compounds. Extracting the intensities from the fitting of a superposition of featureless broad ELNES peaks will fail if the position of the contributing peaks are not known [54]. Here we compare the L edge of different $V^{5+}$, $Mn^{2+}$, $Mn^{3+}$, $Mn^{4+}$ and $Fe^{3+}$ compounds with a different coordination geometry (Fig. 2). Both their ELNES and peak position are very similar at the given resolution suggesting that oxidation state is the dominant parameter to determine shape and position of the L edge for a TM oxide.

Hence, the ELNES fitting method to measure TM oxidation states is generally valid especially when accurate peak positions are used (except when the spin state changes). A similar fitting to our $Mn_3O_4$ ELNES by reference of MnO and $Mn_2O_3$ estimates the average Mn oxidation state as $+2.68(1)$, which is more accurate and precise than the white-line ratio result of $+2.57(6)$ using an exponential fit (Eq. (1)). This method depends on the correct choice of reference spectra [29,31,54,94] and is also applicable to non-integer valence compounds if corresponding reference spectra are available. Recently we even demonstrated direct 2D mapping of Mn oxidation states at atomic resolution in mixed valence compound $Mn_3O_4$ by STEM–EELS using this technique [31].

The ELNES fitting method uses both edge position and ELNES shape to indicate the oxidation state making it more precise and accurate. A large amount of the literature has demonstrated the validity of this method for the $L_{2,3}$ edges of TMs [10,16,78,96]. Absolute peak positions are of primary importance as this forms an essential part of the specificity of the edge especially when sharp characteristic peaks are unavailable [65]. The spectrum at each specimen site can be decomposed as a linear combination of characteristic reference compounds. This is particularly useful to map the distribution of chemical phases, elemental symmetry and oxidation states by 2D scan in STEM–EELS [23,31,32,65,99]. The fitting method should also work for non-integer valence compounds if the corresponding reference is available. Since the ELNES is energy resolution dependent, the better the energy resolution, the more obvious are the characteristic peaks and the higher the confidence level of the fitting result. This is valid in a limited range since the resolution improvement is ultimately limited by the lifetime broadening of the excitation edges ( $\sim 0.1$ eV) [48,98].

It is known that the K edge ELNES can be used as a fingerprint of the crystal symmetry, thus although the ELNES of the TM–L edge is mainly dominated by the oxidation state, minor influences from the crystal symmetry were expected and observed from high energy resolution spectra [16,100]. The ligand and covalency also play a role especially on peak sharpness and relative height [16]. The TM cations of the same oxidation state can also have very different ELNES when they are in different spin states [56,80,81]. All those factors can hinder the application of ELNES fitting to unknown compounds.

Taking into account all the restrictions of the various methods, the chemical shift method at the TM–L edge onset is superior over the white-line ratio method for its wider application range, better consistency, better precision and accuracy and less irregularities (Figs. 4 and 3). With the correct energy position of the excitation edge [55,64], the ELNES fitting method is found to be the best method to measure the oxidation states of TMs from their L edges [31,32]. It is of particular importance to measure the spatial distribution of multiple phases, elemental symmetry or oxidation states by STEM–EELS [31,65,99,101]. These two superior methods demonstrate the importance of the absolute peak position of core-loss excitation edges, especially for relatively featureless ELNES peaks.

## 4. Conclusions

A large group of V/Mn/Fe oxides were systematically investigated to correlate oxidation states to their EELS spectra. The chemical shifts of V/Mn/Fe-$L_{2,3}$ and O–K edges were recorded with high accuracy and their relation to transition metals oxidation states was investigated. The $L_{2,3}$ edges of the transition metals are found to be very similar both in peak shape and energy position for the cations V/Mn/Fe with the same oxidation state. This justifies the validity of fitting the ELNES of unknown compounds with a series of reference spectrum to obtain oxidation state information. The V/Mn-$L_{2,3}$ onset energy is found to linearly relate to the oxidation state of the transition metals.

The white-line ratio method, chemical shift method, edge onset difference method, two-parameter method and ELNES fitting methods are systematically studied and discussed in terms of application range and difficulties. The chemical shift method at the TM–L edge onset is preferred over the white-line ratio method for its wider application range to V/Fe oxides. The ELNES fitting methods is found to be the most applicable method, especially in the case of mixed oxidation states and multiple phases. These two methods demonstrate the importance of the absolute peak position of core-loss excitation edges, which is precisely measured by the script presented here. However, no method exists that can unambiguously and universally determine oxidation states from EELS for all compounds. Great care should be taken in selecting specific methods for different transition elements and cases.

## Acknowledgments

The authors would like to acknowledge the financial support from FWO-Vlaanderen (Project nr. G.0147.06). The authors also acknowledge financial support from the European Research Council under the 7th Framework Program (FP7), ERC Grant No. 46791 - COUNTATOMS and Grant No. NMP3-LA-2010-246102 - IFOX. Thanks to O. Lebedev and Y. Li for providing samples.

## References


[1] J.M.D. Coey, M. Viret, S. von Molnar, Advances in Physics 48 (1999) 167.
[2] T. Wu, et al., Physical Review Letters 86 (2001) 5998.
[3] V. Gold, in: A.D. McNaught, A. Wilkinson (Eds.), Compendium of Chemical Terminology, 2nd ed.,IUPAC, CA, 1997.
[4] R.S. Mulliken, Journal of Chemical Physics 23 (1955) 1833.
[5] R.F.W. Bader, Atoms in Molecules: A Quantum Theory, Clarendon Press, Oxford, 1994.
[6] G. Henkelman, A. Arnaldsson, H. Jonsson, Computational Materials Science 36 (2006) 354.
[7] K.J. Vetter, N. Jaeger, Electrochimica Acta 11 (1966) 401.
[8] J.A. Lee, C.E. Newnham, F.S. Stone, F.I. Tye, Journal of Solid State Chemistry 31 (1980) 81.
[9] J. Wong, F.W. Lytle, R.P. Messmer, D.H. Maylotte, Physical Review B 30 (1984) 5596.
[10] B. Gilbert, et al., Journal of Physical Chemistry A 107 (2003) 2839.
[11] J. Lee, et al., Physical Review B 80 (2009) 205112.
[12] R.S. Liu, et al., Journal of Solid State Chemistry 128 (1997) 326.
[13] S.M. Mini, et al., in: Science and Technology of Magnetic Oxides, Cambridge, Boston, 1998.
[14] H.K. Schmid, W. Mader, Micron 37 (2006) 426.
[15] C.C. Ahn (Ed.), Transmission electron energy-loss spectrometry in materials science and the EELS atlas, 2nd ed.,Wiley, Darmstadt, 2004.
[16] L. Garvie, A. Craven, Physics and Chemistry of Minerals 21 (1994) 191.
[17] J.H. Rask, B.A. Miner, P.R. Buseck, Ultramicroscopy 21 (1987) 321.
[18] L. Kourkoutis, et al., Physical Review Letters 97 (2006) 256803.
[19] T. Daulton, B. Little, Ultramicroscopy 106 (2006) 561.
[20] Z.L. Wang, J. Bentley, N.D. Evans, Micron 31 (2000) 355.
[21] A.M. Arevalo-Lopez, M.A. Alario-Franco, Inorganic Chemistry 48 (2009) 11843.
[22] C. Colliex, T. Manoubi, C. Ortiz, Physical Review B 44 (1991) 11402.
[23] L. Cave, et al., Micron 37 (2006) 301.
[24] D. Loomer, T. Al, L. Weaver, S. Cogswell, American Mineralogist 92 (2007) 72.
[25] T. Riedl, T. Gemming, K. Wetzig, Ultramicroscopy 106 (2006) 284.
[26] J.H. Paterson, O.I. Krivanek, Ultramicroscopy 32 (1990) 319.
[27] C.T. Meneses, M.A. Macedo, F.C. Vicentin, Journal of Electron Spectroscopy and Related Phenomena 156 (2007) 326.
[28] A. Gloter, et al., European Physical Journal B 22 (2001) 179.
[29] L. Garvie, P.R. Buseck, Nature 396 (1998) 667.
[30] G. Botton, C. Appel, A. Horsewell, W. Stobbs, Journal of Microscopy 180 (1995) 211.
[31] H. Tan, et al., Physical Review Letters 107 (2011) 107602.
[32] S. Turner, et al., Nanoscale 3 (2011) 3385.
[33] K. Suenaga, M. Koshino, Nature 468 (2010) 1088.
[34] M. Varela, et al., Physical Review B 79 (2009) 085117.
[35] Y. Suchorski, et al., Applied Surface Science 249 (2005) 231.
[36] P.A. van Aken, B. Liebscher, Physics and Chemistry of Minerals 29 (2002) 188.
[37] J. Graetz, et al., Physical Review B 69 (2004) 235103.
[38] S. Oswald, K. Nikolowski, H. Ehrenberg, Surface and Interface Analysis 42 (2010) 916.
[39] G. Logvenov, A. Gozar, I. Bozovic, Science 326 (2009) 699.
[40] A. Ohtomo, H.Y. Hwang, Nature 427 (2004) 423.
[41] R.D. Leapman, L.A. Grunes, Physical Review Letters 45 (1980) 397.
[42] F.M.F. de Groot, J.C. Fuggle, B.T. Thole, G.A. Sawatzky, Physical Review B 41 (1990) 928.
[43] T. Riedl, et al., Micron 38 (2007) 224.
[44] P.A. van Aken, B. Liebscher, V.J. Styrsa, Physics and Chemistry of Minerals 25 (1998) 323.
[45] T.G. Sparrow, B.G. Williams, C.N.R. Rao, J.M. Thomas, Chemical Physics Letters 108 (1984) 547.
[46] B.K. Agarwal, L.P. Verma, Journal of Physics C: Solid State Physics 3 (1970) 535.
[47] J. Taftø, O.L. Krivanek, Physical Review Letters 48 (1982) 560.
[48] R.F. Egerton, Electron Energy-Loss Spectroscopy in the Electron Microscope, 3rd ed., Springer, New York, 2011.
[49] F.A. Gianturco, C.A. Coulson, Molecular Physics 14 (1968) 223.
[50] M.N. Ghatikar, B.D. Padalia, Journal of Physics C: Solid State Physics 11 (1978) 1941.
[51] M. Tromp, J. Moulin, G. Reid, J. Evans, X-Ray Absorption Fine Structure—XAFS13, AIP, New York, 2007.
[52] G. van der Laan, L.W. Kirkman, Journal of Physics—Condensed Matter 4 (1992) 4189.
[53] N. Nakagawa, H.Y. Hwang, D.A. Muller, Nature Materials 5 (2006) 204.
[54] S. Zhang, et al., American Mineralogist 95 (2010) 1741.
[55] P. Potapov, D. Schryvers, Ultramicroscopy 99 (2004) 73.
[56] S.P. Cramer, et al., Journal of the American Chemical Society 113 (1991) 7937.
[57] Y. Sasano, S. Muto, Journal of Electron Microscopy 57 (2008) 149.
[58] B. Jouffrey, P. Schattschneider, C. Hébert, Ultramicroscopy 102 (2004) 61.
[59] C. Hébert, P. Schattschneider, H. Franco, B. Jouffrey, Ultramicroscopy 106 (2006) 1139.
[60] 〈www.felmi-zfe.tugraz.at/dm_scripts〉.
[61] J.A. Hunt, D.B. Williams, Ultramicroscopy 38 (1991) 47.
[62] M. Bosman, V. Keast, Ultramicroscopy 108 (2008) 837.
[63] R. Egerton, P. Li, M. Malac, Micron 35 (2004) 399.
[64] A. Gubbens, et al., Ultramicroscopy 110 (2010) 962.
[65] J. Angseryd, M. Albu, H.O. Andrén, G. Kothleitner, Micron 42 (2011) 608.
[66] Y. Li, et al., Small 7 (2011) 475.
[67] Y. Li, et al., Crystal Growth & Design 10 (2010) 2969.
[68] A. Abakumov, et al., Journal of Solid State Chemistry 182 (2009) 2231.
[69] V. Caignaert, et al., Chemistry of Materials 21 (2009) 1116.
[70] H. D'Hondt, et al., Chemistry of Materials 20 (2008) 7188.
[71] H. Horowitz, J. Longo, Materials Research Bulletin 13 (1978) 1359.
[72] T. Negas, R. Roth, Journal of Solid State Chemistry 1 (1970) 409.
[73] S. Mori, Journal of the American Ceramic Society 49 (1966) 600.
[74] C. Turquat, et al., International Journal of Inorganic Materials 3 (2001) 1025.
[75] H. Kurata, C. Colliex, Physical Review B 48 (1993) 2102.
[76] C. Mitterbauer, et al., Ultramicroscopy 96 (2003) 469.
[77] R.D. Leapman, P. Rez, D.F. Mayers, Journal of Chemical Physics 72 (1980) 1232.
[78] F.M.F. de Groot, J.C. Fuggle, B.T. Thole, G.A. Sawatzky, Physical Review B 42 (1990) 5459.
[79] R. Leapman, L. Grunes, P. Fejes, Physical Review B 26 (1982) 614.
[80] B.T. Thole, G. van der Laan, Physical Review B 38 (1988) 3158.
[81] D.M. Pease, et al., Physics Letters A 114 (1986) 491.
[82] H. Kurata, N. Tanaka, Microscopy Microanalysis Microstructures 2 (1991) 183.
[83] K. Chen, et al., Micron 38 (2007) 354.
[84] T. Daulton, B. Little, K. Lowe, J. Jones-Meehan, Journal of Microbiological Methods 50 (2002) 39.
[85] Z.L. Wang, J.S. Yin, Y.D. Jiang, Micron 31 (2000) 571.
[86] P. Rez, Ultramicroscopy 9 (1982) 283.
[87] W. Hai-Ping, et al., Chinese Physics B 18 (2009) 5008.
[88] D.H. Pearson, C.C. Ahn, B. Fultz, Physical Review B 47 (1993) 8471.
[89] L. Garvie, A. Craven, Ultramicroscopy 54 (1994) 83.
[90] H.D. Zhou, J.B. Goodenough, Journal of Solid State Chemistry 178 (2005) 3679.
[91] J. Gopalakrishnan, C.N.R. Rao, New Directions in Solid State Chemistry, Cambridge University Press, Cambridge, 1997.
[92] T. Kataoka, et al., Applied Physics Letters 96 (2010) 252502.
[93] V. Bhide, R. Dani, Physica 27 (1961) 821.
[94] L. Laffont, P. Gibot, Materials Characterization 61 (2010) 1268.
[95] L. Garvie, P. Buseck, A. Craven, Canadian Mineralogist 33 (1995) 1157.
[96] L. Garvie, A. Craven, R. Brydson, American Mineralogist 79 (1994) 411.
[97] G. van der Laan, B.T. Thole, G.A. Sawatzky, M. Verdaguer, Physical Review B 37 (1988) 6587.
[98] F. de Groot, A. Kotani, Core Level Spectroscopy of Solid, CRC Press, Boca Raton, 2008.
[99] S. Turner, et al., submitted for publication.
[100] R. Brydson, et al., Journal of Physics—Condensed Matter 5 (1993) 9379.
[101] L. Monico, et al., Analytical Chemistry 83 (2011) 1214.